


Artificial Cell-Derived Vesicles: Extracellular Vesicle Mimetics for Chondrocyte Restoration in TMJOA Therapy

Yu Hu^{1,*}, Guobin Huang^{2,3,*}, Zichao Dai^{2,3}, Rongqiang Yang^{2,3}, Yang Zhang⁴, Yelin Zhang^{2,3}, Huilin Shen^{2,3}, Zhu Pu^{2,3}, Liya Ma^{2,3}, Song Li^{2,3}

¹Outpatient Department, Kunming Medical University School and Hospital of Stomatology, Kunming, 650106, People's Republic of China; ²Yunnan Key Laboratory of Stomatology, Kunming, 650106, People's Republic of China; ³Department of Dental Research, Kunming Medical University School and Hospital of Stomatology, Kunming, 650106, People's Republic of China; ⁴Stomatology Center of Baoshan People's Hospital, Baoshan, Yunnan, 678000, People's Republic of China

*These authors contributed equally to this work

Correspondence: Liya Ma; Song Li, Email 20211733@kmmu.edu.cn; lisong@kmmu.edu.cn

Purpose: Cartilage repair in temporomandibular joint osteoarthritis (TMJOA) remains a clinical challenge. Despite the strong repair potential of extracellular vesicles (EVs), their clinical use is constrained by yield and purification issues. This study explores artificial cell-derived vesicles (ACDVs) as a novel acellular strategy for cartilage repair, providing a promising alternative to EVs.

Methods: EVs and ACDVs were isolated from umbilical cord mesenchymal stem cells, and their particle number and protein yield were compared. Mandibular condylar chondrocytes (MCCs) were treated with EVs/ACDVs after IL-1 β stimulation to assess their effects on MCC apoptosis, proliferation, migration, and chondrogenic differentiation. Transcriptomic analysis was conducted to explore the therapeutic mechanisms of ACDVs. In a rat TMJOA model, local ACDV injection was evaluated for its effects on cartilage matrix synthesis and subchondral bone repair.

Results: ACDVs resembled EVs in morphology and particle size, but exhibited significantly higher particle counts and protein yields. Efficiently internalized by MCCs, ACDVs effectively mitigated IL-1 β -induced apoptosis, while promoting MCC proliferation, migration, and chondrogenic differentiation. This effect was likely mediated by the activation of genes involved in extracellular matrix synthesis. In a rat model of TMJOA, local ACDV injection ameliorated subchondral bone damage and stimulated cartilage matrix synthesis.

Conclusion: This study demonstrates that ACDVs, generated by stepwise extrusion, are produced at significantly higher yields than EVs and show equal or superior efficacy in cartilage matrix repair. These findings endorse ACDVs as a promising alternative to EVs for disease therapy and drug delivery.

Keywords: artificial cell-derived vesicles, extrusion-derived vesicles, temporomandibular joint osteoarthritis, chondrocytes

Introduction

Osteoarthritis (OA) is the most common musculoskeletal disorder in individuals over 60 years old, characterized by cartilage matrix degradation, articular cartilage degeneration, synovial inflammation, and osteophyte formation.¹ Temporomandibular joint osteoarthritis (TMJOA), a major form of temporomandibular joint disorders, causes limited mouth opening, chewing dysfunction, and chronic pain in the joint and surrounding musculature, profoundly impairing quality of life.^{2,3} The reported prevalence of TMJOA among patients with temporomandibular disorders ranges from 18.0% to 84.7%.^{4,5} Current “graded sequential treatments” for TMJOA primarily address pain, stiffness, and swelling but fail to regenerate cartilage or restore joint homeostasis, underscoring the urgent need for novel therapeutic strategies.⁶

The regenerative capacity of articular cartilage is markedly diminished by its avascular and aneural nature, low chondrocyte density, and immune dysregulation induced by inflammation.⁷ Bioactive materials, including hydrogels, 3D scaffolds, nanomaterials, and extracellular vesicles (EVs), are widely employed in OA treatment, among which EVs have

gained significant attention as a highly promising therapeutic strategy owing to their superior biocompatibility and unique cell-free properties.^{8–11} As critical mediators of paracrine signaling, EVs transfer bioactive molecules between cells, reprogramming signaling networks and modulating host cell functions, thereby playing a pivotal role in disease management.¹² Numerous studies have demonstrated that EVs promote OA cartilage repair by regulating chondrocyte differentiation, modulating inflammation and immune responses, and enhancing cartilage matrix synthesis.^{13–15} Our previous work demonstrated that EVs derived from mesenchymal stem cells can restore chondrocyte function in the condyle under inflammatory conditions, facilitating cartilage repair in a rat TMJOA model. However, the high cost, low yield, and complex isolation processes of EVs pose significant barriers to their clinical application.^{16,17} Thus, engineering EVs to enhance their functionality, or developing vesicle-like structures with analogous properties, is crucial for their future therapeutic applications.

Artificial cell-derived vesicles (ACDVs) are nanoscale, synthetic vesicles designed to mimic the characteristics and functions of natural extracellular vesicles. Through bioengineering, these vesicles can be optimized for specific biomedical applications. Compared to their naturally derived counterparts, ACDVs offer superior control, stability, and production efficiency, making them promising candidates for drug delivery, disease therapy, and regenerative medicine.^{18,19} Current fabrication techniques, including ultrasound, PH gradient methods, microfluidics, electroporation, and stepwise extrusion, are widely used for vesicle preparation and drug encapsulation.²⁰ Stepwise extrusion, owing to its simplicity and ease of use, has attracted considerable attention. ACDVs generated by this method yield over 20 times the amount of EVs, maintaining membrane structures akin to those of the parent cells, containing cellular contents, and demonstrating therapeutic potential similar to that of both the parent cells and EVs.²¹ Zhang et al conducted proteomic analysis of EVs derived from human umbilical mesenchymal stem cells (UCMSCs) and extrusion-derived vesicles, finding that ACDVs exhibit EV-like membrane structures, comparable particle sizes, and a significantly higher protein content.²²

This study seeks to address the dose-effect challenges in EV applications, with a particular focus on the development and therapeutic potential of ACDVs for treating TMJOA. ACDVs will be produced via stepwise extrusion, and their capacity to maintain chondrocyte function in inflammatory environments, as well as their impact on cartilage matrix synthesis and repair in TMJOA, will be evaluated. This research aims to provide novel insights into overcoming the yield limitations of EVs, laying the groundwork for acellular therapies based on ACDVs in the treatment of TMJOA and potentially systemic osteoarthritis.

Materials and Methods

Cell Culture and Characterization

The primary culture of mandibular condylar chondrocytes (MCCs) was approved by the Animal Ethics Committee of Kunming Medical University (KMMU 20240172) and conducted in strict compliance with the 3R principles (Replacement, Reduction, Refinement). Briefly, mandibular condyles from neonatal Sprague-Dawley rats were dissected, minced, and digested with 0.2% type II collagenase (Sigma, USA) at 37°C for 30 minutes. The dissociated cells were cultured in high-glucose DMEM (Biological Industries, Israel) containing 20% fetal bovine serum (FBS; Biological Industry). Toluidine blue staining and COL2 immunofluorescence were performed to identify MCCs. Umbilical cord mesenchymal stem cells (UCMSCs) were purchased from Haixin Biological Co., Ltd. (UCHX-C106; Suzhou, China).

Isolation and Characterization of EVs and ACDVs

UCMSCs were seeded in 225 cm² culture flasks at a density of 1×10^6 cells/flask and cultured in Umibio[®] Serum-free MSC media (China) upon reaching 60% confluence. After 48 h, the UCMSCs supernatant was collected for EV isolation, while the cells were harvested for ACDVs preparation. Briefly, the supernatant was centrifuged at 12,000 g for 30 min at 4°C to remove protein aggregates, and passed through a 0.22 µm filter to exclude microvesicles and apoptotic bodies. The clarified supernatant was loaded into the EXODUS automated purification system (Huixin Lifetech, China) with an A03M chip and processed using the CM.Strong-MA.A03 program. Purified EVs were resuspended in phosphate buffer solution (PBS; Beyotime, China). UCMSCs were enzymatically dissociated and resuspended in PBS. The cell suspension was sequentially filtered through 10 µm, 1 µm, and 0.4 µm Nuclepore membranes (Whatman, UK), followed by 0.22 µm

filtration. The filtrate was concentrated using a 100 kDa ultrafiltration tube (Millipore, USA) by centrifugation at 5000 g for 30 min at 4°C, and ACDVs were collected from the upper chamber.

The protein concentration of EVs and ACDVs was quantified by bicinchoninic acid (BCA; Beyotime) assay. To characterize EVs and ACDVs, transmission electron microscopy (TEM; Hitachi, Japan) was used to visualize morphology, particle size and zeta potential were measured with a ZetaView PMX110 (Particle Metrix, Germany). Protein distribution was assessed via Coomassie Brilliant Blue staining in EVs, ACDVs, and their parent UCMSCs, while Western blotting detected CD81, HSP90, and TSG101 expression. Particle concentration and protein content of UCMSC-derived EVs and ACDVs were quantified and compared.

Internalization of EVs and ACDVs by MCCs

EVs and ACDVs were labeled with PKH67 (Sigma) following the manufacturer's protocol and co-cultured with MCCs. At 3, 12, and 24 h post-incubation, cells were fixed and stained with phalloidin-Atto 647N (Sigma) to visualize the cytoskeleton. The internalization of EVs and ACDVs was assessed via confocal microscopy (Nikon, Japan), and uptake rates were quantified by flow cytometry (Agilent Technologies, USA).

Apoptosis Assay

MCCs (5×10^5 cells/well) were seeded in six-well plates and cultured to 60% confluence, serum-starved for 12 h, and treated with 10 ng/mL IL-1 β for 24 h. Following IL-1 β exposure, cells were incubated with 50 μ g/mL EVs or ACDVs for an additional 24 h. Cells were then harvested using EDTA-free trypsin, resuspended in Binding Buffer, and stained with Annexin V-FITC and PI (KGI Biotechnology, China) for 15 minutes at room temperature in the dark. Flow cytometry analysis was performed within 1 h using 488 nm excitation.

Proliferation Assay

MCCs were seeded at 2000 cells per well in 96-well plates and serum-starved overnight. After 24 h of IL-1 β treatment (10 ng/mL), cells were exposed to EVs or ACDVs (50 μ g/mL). At days 1, 2, 4, and 6, cells were incubated with CCK-8 solution (MeilunBio, China) for 2 h in the dark, and absorbance at 450 nm was measured. Following the above treatment conditions, total protein was extracted from the cells, and proliferation markers PCNA and MCM7 were analyzed via Western blotting.

Migration Assay

MCCs (5×10^4 cells) were seeded in Culture-Insert (Ibidi, Germany), which were removed the next day. Following PBS washing, cells were cultured in serum-free medium, serum-free medium with 50 μ g/mL EVs, or serum-free medium with 50 μ g/mL ACDVs. Cell migration was monitored and images captured at 0, 6, 12, and 24 h.

Chondrogenic Differentiation Assay

MCCs were cultured in chondrogenic induction medium (Cyagen, China) with IL-1 β to establish an inflammatory microenvironment, followed by treatment with EVs and ACDVs. On day 7, cells were fixed and stained with Alcian Blue, and images were captured using an inverted phase contrast microscope. Western blotting was performed to quantify the expression of chondrogenic markers sox9 and COL2.

Western Blot

Cells, EVs, and ACDVs samples were lysed at low temperature to extract total protein, quantified by BCA assay. After heat denaturation, proteins were resolved by SDS-PAGE and transferred onto membranes (Invitrogen system, Thermo Fisher Scientific, USA). Membranes were blocked with Beyotime blocking solution (30 min, room temperature), incubated with primary antibodies overnight at 4°C, and then with secondary antibodies for 90 min at room temperature. Signal detection was carried out using BeyoECL Star (Beyotime). Antibody details are listed in [Table S1](#).

For Coomassie Brilliant Blue staining, protein samples were electrophoresed, stained with Coomassie Blue Staining Solution (Beyotime) at room temperature for 1 h, washed, and imaged.

RNA Sequencing and Analysis

MCCs were divided into four groups: Control, IL-1 β , EVs + IL-1 β , and ACDVs + IL-1 β . Total RNA was extracted, libraries constructed, and sequenced on a high-throughput platform to obtain raw data. Gene alignment and quality control were performed with SRATsolo, producing a count matrix. Principal component analysis (PCA) was conducted using the *prcomp* function in R. Differentially expressed genes (DEGs) between the IL-1 β and Control groups were identified using DESeq2, with significance set at $P < 0.05$. Inflammation-related gene sets were retrieved from Hallmark, C2 (curated gene sets), and C5 (ontology gene sets) in gsea-msigdb, filtered for the rat species, resulting in 3843 inflammation-associated genes, designated as the *inflammation* gene set. This gene set was then intersected with the differentially expressed genes between the IL-1 β and Control groups. Differential gene analysis for “IL-1 β _EVs” vs “IL-1 β ” and “IL-1 β _ACDVs” vs “IL-1 β ” was conducted with thresholds of $P < 0.05$ and $|\log FC| > 1$. Enrichment analyses for KEGG and GO pathways were performed on the gene lists using *ClusterProfiler*, while heatmaps and hierarchical clustering of target genes were generated with *pheatmap*.

Animal Experiments

This study was approved by the Animal Ethics Committee of Kunming Medical University (KMMU 20240172). Healthy male Sprague-Dawley rats (200–250 g, 8 weeks old) were used to establish a bilateral TMJOA model through anterior crossbite induction. Maxillary metal tubes (3–5 mm) and mandibular tubes (8–10 mm, angled 135° labially) were crafted from 13-gauge syringe needles. After routine disinfection and anesthesia (3% pentobarbital sodium, 1 mL/kg), the incisors were dried, acid-etched, and fitted with metal tubes on the left maxillary and mandibular incisors using 3M ESPE Relyx U200 self-adhesive resin cement, then light-cured for 40s. Rats were maintained in anterior crossbite for four weeks to induce TMJOA. Subsequently, 100 μ g of PBS, EVs, or ACDVs was administered weekly via intra-articular injections into the left TMJ, with samples collected at 2, 4, and 8 weeks post-treatment.

Micro-CT Analysis

Left TMJs were harvested from all rats, fixed in 4% paraformaldehyde for 24 h, and scanned with a NEMO[®] NMC-100 micro-CT system (90 kV, 60 μ A). Reconstructed images (Avatar 1.5.0) enabled comparative analysis of subchondral bone degradation across groups. Quantitative parameters included trabecular number (Tb.N), trabecular separation (Tb.Sp), and bone volume fraction (BV/TV).

Histological Analysis

After fixation, decalcification, and dehydration, samples were embedded in paraffin, sectioned at 4 μ m, and stained with hematoxylin-eosin (HE) and Safranin O–Fast Green. Immunohistochemistry (IHC) was conducted to evaluate sox9 and COL2 expression in the cartilage matrix. Slides were scanned (KF-PRO-005, KFBIO, China) and analyzed for sox9 and COL2 positivity using K-viewer 1.7.0.27.

Statistical Analysis

Statistical analyses and figure preparation were conducted in GraphPad Prism 10. For normally distributed data, independent sample *t*-tests (two groups) and one-way ANOVA (three or more groups) were applied. For non-normally distributed data, nonparametric tests (two groups) and Kruskal–Wallis tests (three or more groups) were used. Significance was defined as $P < 0.05$.

Results

Characterization of EVs and ACDVs

EVs and ACDVs derived from UCMSCs displayed comparable saucer-like morphology (Figure 1A), with diameters around 120 nm (EVs: 120.9 nm; ACDVs: 120.5 nm; Figure 1B) and stable Zeta potentials (EVs: −36.50 mV; ACDVs: −36.99 mV; Figure 1C). Protein profiles in both EVs and ACDVs resembled those of parental cells, primarily at 10–15 kD and 70 kD (Figure 1D). Notably, ACDVs were enriched in TSG101 and HSP90, whereas EVs prominently expressed CD81 (Figure 1E).

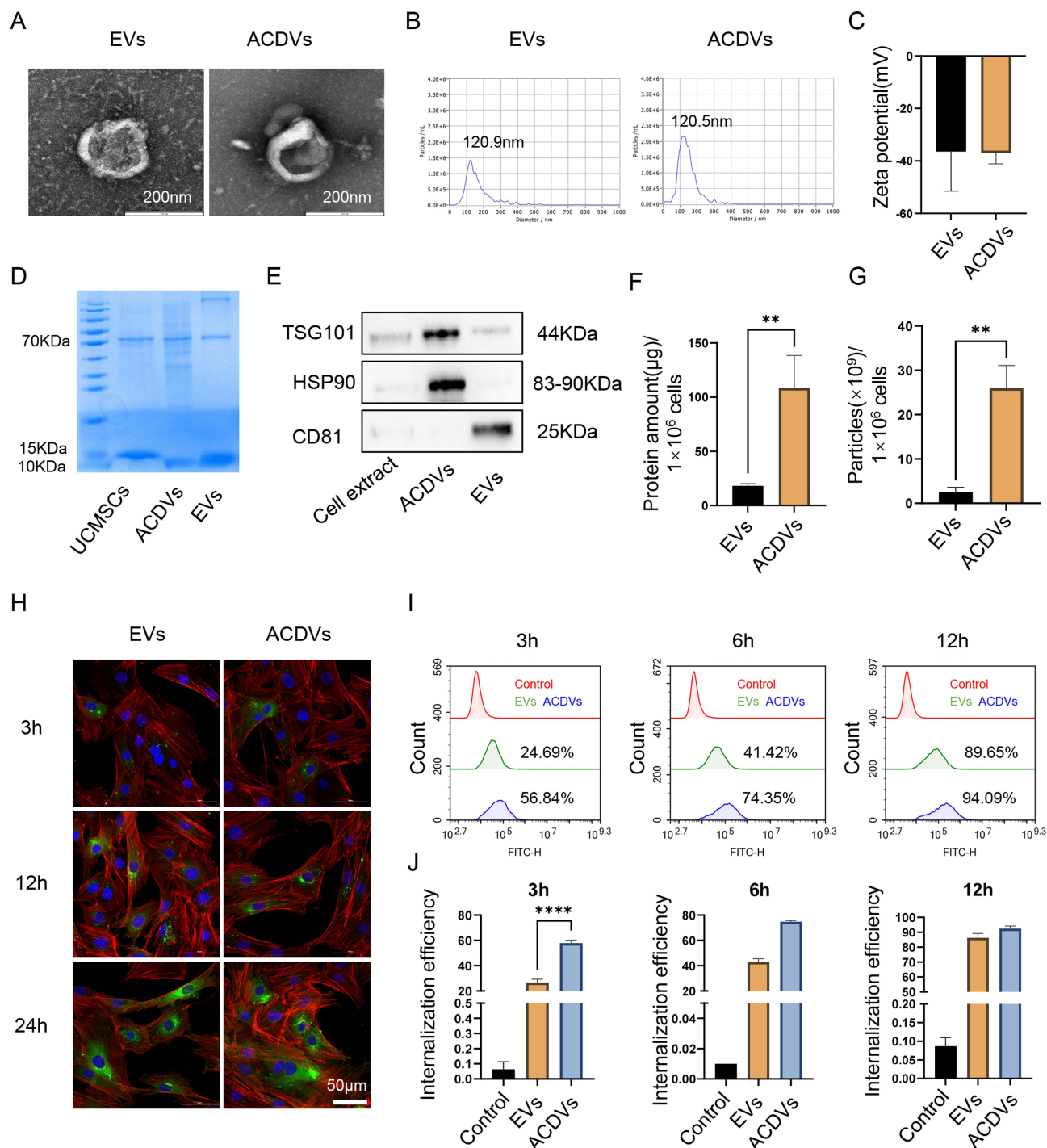


Figure 1 Characterization of EVs and ACDVs. **(A)** TEM images showing EV and ACDV morphology. Scale bar = 200 nm. **(B)** Particle size distribution of EVs and ACDVs. **(C)** Zeta potential measurements of EVs and ACDVs. $n = 3$. **(D)** The protein distribution of EVs and ACDVs. **(E)** Western blot analysis of EV markers, including CD81, HSP90, and TSG101. **(F)** Protein yields from EVs and ACDVs derived from equivalent UCMSC quantities. $n = 3$. **(G)** Particle counts of EVs and ACDVs produced by equivalent UCMSC quantities. $n = 3$. **(H)** Confocal imaging of EV/ACDV uptake by MCCs. MCC nuclei stained with DAPI (blue), EVs/ACDVs with PKH67 (green), and the cytoskeleton with phalloidin (red). Scale bar = 50 μm . **(I)** Flow cytometry analysis of EV/ACDV uptake by MCCs. **(J)** Quantification of uptake rates. $n = 3$. ** $P < 0.01$; **** $P < 0.0001$.

Yield analysis showed that equivalent amounts of UCMSCs generated significantly more ACDVs than EVs, with ACDVs showing 5.95-fold higher protein yields (Figure 1F) and 11.76-fold higher particle counts (Figure 1G).

To evaluate MCC uptake of ACDVs, PKH67-labeled EVs and ACDVs were separately co-cultured with MCCs. Confocal microscopy revealed faint green fluorescence around the nuclei and in the cytoplasm of MCCs at 3 h, with the

uptake of both EVs and ACDVs increasing over time (Figure 1H). Flow cytometry showed significantly higher ACDVs uptake by MCCs compared to EVs at 3 h, with both reaching saturation by 12 h (Figure 1I and J).

The Effects of EVs and ACDVs on MCC Biological Functionality

Primary MCCs displayed a distinct “cobblestone” growth pattern (Figure S1A), transitioning to a spindle-like morphology with dedifferentiation upon passaging (Figure S1B). Chondrogenic identity was confirmed by positive Toluidine blue staining (Figure S1C) and type II collagen (COL2) immunofluorescence (Figure S1D).

Flow cytometry demonstrated that 10 ng/mL IL-1 β induced MCC apoptosis, while 50 μ g/mL of either EVs or ACDVs significantly mitigated apoptosis under inflammatory conditions (Figure 2A and B). CCK-8 assays revealed that both EVs and ACDVs substantially promoted MCC proliferation, with ACDVs showing a notably higher effect than EVs on day 2. By day 4, proliferation rates had plateaued across groups, narrowing intergroup differences (Figure 2C). Western blot analysis further indicated that IL-1 β suppressed the expression of proliferation markers PCNA and MCM7, an effect that was reversed by EVs and ACDVs (Figure 2D and E). Wound healing assays demonstrated that both EVs and ACDVs effectively promoted MCC migration, achieving complete closure by 24 h (Figure 2F and G). Chondrogenic induction experiments demonstrated that IL-1 β significantly inhibited chondrogenic differentiation in MCCs, leading to varying degrees of downregulation of the matrix proteins COL2 and sox9. Both EVs and ACDVs effectively restored the suppressed expression of these proteins; however, ACDVs uniquely rescued the impaired chondrogenic differentiation capacity of MCCs compared to EVs (Figure 2H and I).

RNA Sequencing and Analysis

PCA revealed consistent gene expression patterns within treatment groups and distinct profiles between groups, underscoring intervention stability (Figure 3A). Using an IL-1 β -induced inflammatory cartilage model, we identified 153 IL-1 β -responsive inflammation-related genes by intersecting differentially expressed genes from the IL-1 β vs Control comparison with the inflammation gene set (Figure 3B). We further examined the effects of EVs and ACDVs treatments compared to untreated inflammatory group. In the “IL-1 β _EVs” vs “IL-1 β ” comparison, 516 DEGs were identified ($P < 0.05$, $|\log FC| > 1$), with 191 downregulated and 325 upregulated (Figure 3C). In the “IL-1 β _ACDVs” vs “IL-1 β ” comparison, 1206 DEGs were detected, comprising 535 downregulated and 671 upregulated genes (Figure 3E). KEGG enrichment analysis of DEGs highlighted significant activation of inflammatory pathways, including TNF, NF- κ B, chemokine signaling, and rheumatoid arthritis pathways, under cartilage inflammation (Figure 3D and F). To compare the therapeutic effects of the two vesicle types, we analyzed DEGs between “IL-1 β _ACDVs” and “IL-1 β _EVs”, identifying 149 DEGs, with 57 downregulated and 92 upregulated (Figure 3G). To delineate pathway differences between the two vesicle treatments, enrichment analysis of the 149 DEGs identified key associations with extracellular matrix and inflammatory processes (Figure 3H). Heatmap analysis of extracellular matrix-related genes demonstrated that IL-1 β _ACDVs more robustly activated these genes compared to IL-1 β _EVs, aligning with our earlier findings (Figure 3I). Hierarchical clustering of the 153 key genes across the four groups revealed distinct expression patterns. Notably, 38 inflammation-related genes, including *Enpp1*, were significantly upregulated upon IL-1 β induction and markedly downregulated following vesicle treatment, with ACDVs showing greater suppression than EVs. This gene subset may represent key therapeutic targets for vesicle-based interventions in cartilage inflammation (Figure 3J). GO enrichment analysis indicated these genes are involved in the negative regulation of cartilage differentiation and development (Figure 3K).

EVs and ACDVs Facilitated Cartilage and Subchondral Bone Repair in TMJOA

Micro-CT revealed that the condyle in TMJOA rats was porous and rough. Following treatment with EVs and ACDVs, the trabecular bone showed increased density and a smoother surface (Figure 4A). Quantitative analysis indicated that, at 2 weeks post-surgery, the PBS-injected group exhibited a significant reduction in Tb. BV/TV and Tb. N in the subchondral bone compared to the Blank group. In contrast, ACDVs treatment significantly repaired the damaged subchondral bone, as shown by increased Tb. N and decreased Tb. Sp at 4 weeks, followed by elevated Tb. BV/TV at 8 weeks (Figure 4B). These results demonstrated that ACDVs exert a reparative effect on the damaged subchondral bone in TMJOA rats.

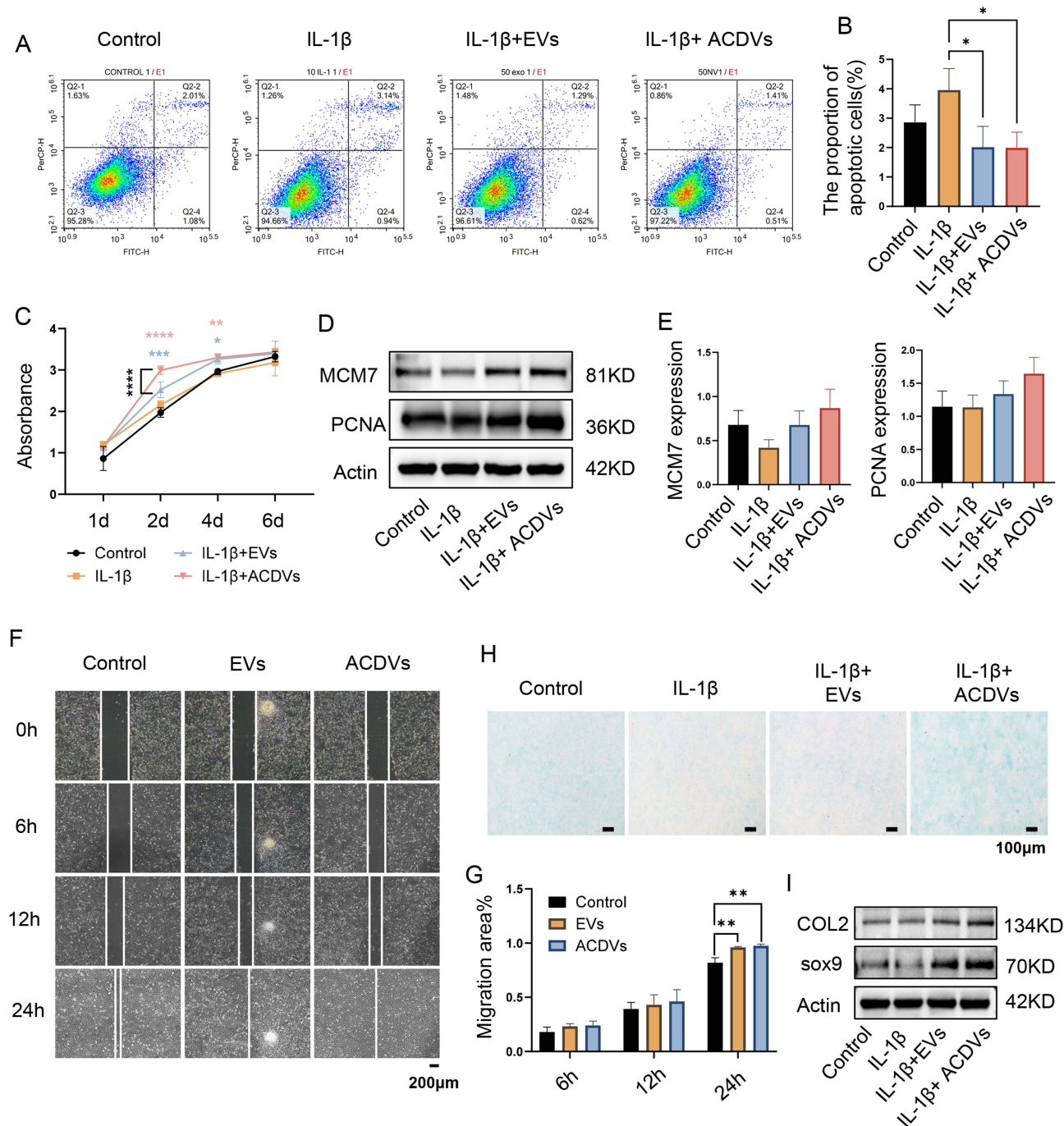


Figure 2 The effects of EVs and ACDVs on the biological functions of MCCs. **(A)** Flow cytometry assessing the effects of EVs/ACDVs on MCC apoptosis levels. **(B)** Quantitative analysis of apoptosis rates. $n = 3$. **(C)** CCK-8 assay evaluating EV/ACDVs effects on MCC proliferation. $n = 6$. **(D)** Western blot of proliferation markers (MCM7, PCNA) in MCCs after EV/ACDVs treatment. **(E)** Quantitative protein expression analysis. $n = 3$. **(F)** Scratch assay to assess the effects of EVs/ACDVs on MCC migration. **(G)** Quantitative analysis of migration rates. $n = 3$. **(H)** Alcian blue staining for chondrogenic differentiation of MCCs after EV/ACDVs exposure. **(I)** Western blot of chondrogenic matrix proteins (sox9, COL2) in MCCs treated with EVs/ACDVs. * $P < 0.05$; ** $P < 0.01$; *** $P < 0.001$; **** $P < 0.0001$.

Histological staining showed disorganized cartilage layers, reduced collagen density, fewer hypertrophic chondrocytes, and increased inflammatory cell infiltration in TMJOA rat condyles. In contrast, EVs and ACDVs treatment reduced inflammatory infiltration, increased hypertrophic chondrocytes, restored cartilage organization, and improved subchondral bone structure (Figures 4C and S2). Mankin scores for the EVs and ACDVs groups were significantly lower than those for PBS, indicating partial restoration of cartilage integrity in TMJOA (Figure 4D).

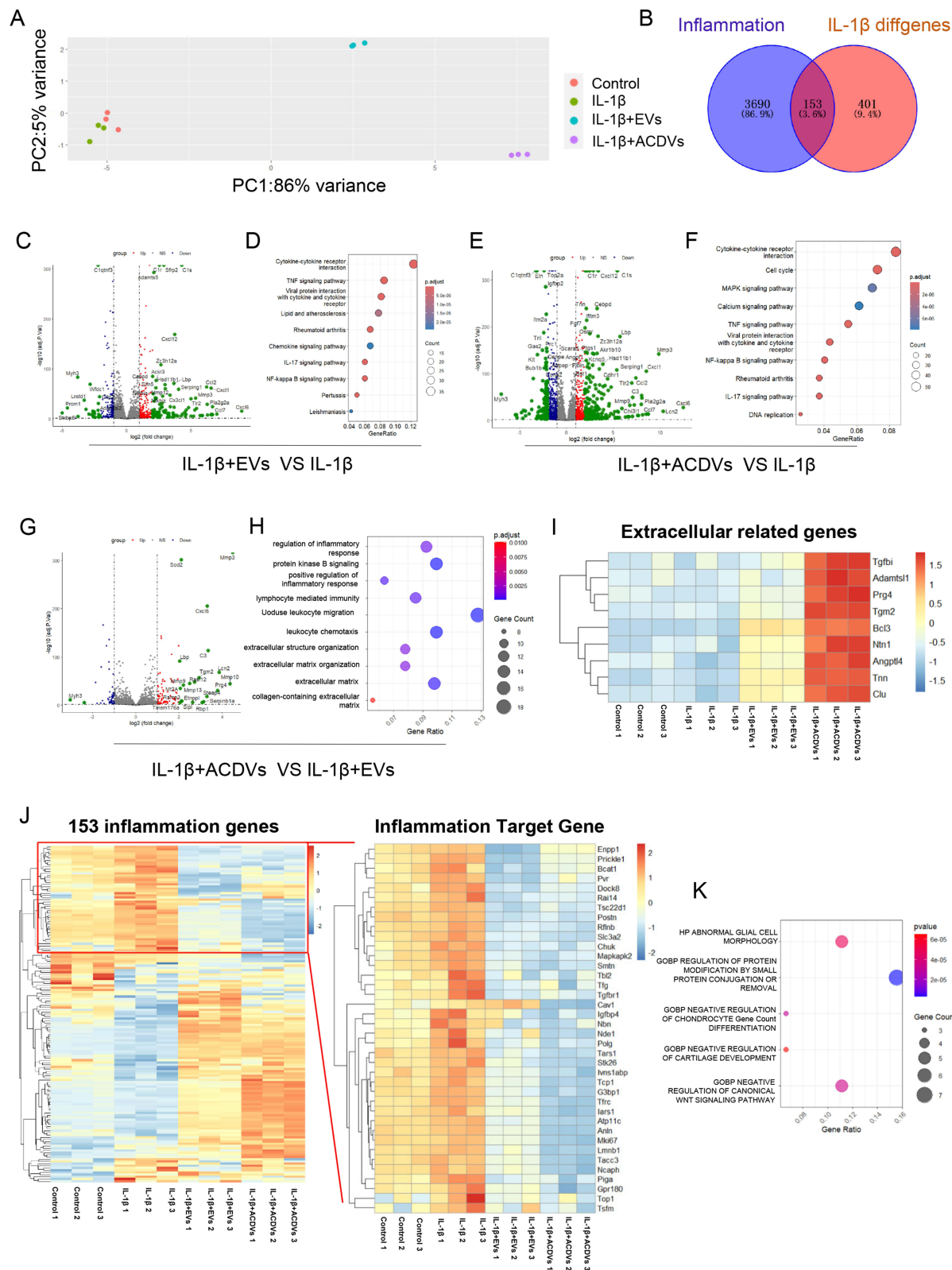


Figure 3 RNA sequencing and analysis. **(A)** PCA in all groups. **(B)** Intersection of DEGs between the IL-1 β and Control groups with inflammation-related genes. **(C and D)** Volcano plots and KEGG pathway enrichment of DEGs between the IL-1 β + EVs and IL-1 β groups. **(E and F)** Volcano plots and KEGG pathway enrichment of DEGs between the IL-1 β + ACDVs and IL-1 β groups. **(G and H)** Volcano plots and KEGG pathway enrichment of DEGs between the IL-1 β + ACDVs and IL-1 β + EVs groups. **(I)** Heatmap of extracellular matrix-related genes across groups. **(J)** Heatmap of inflammation-related genes across groups. **(K)** GO enrichment analysis of inflammation-related genes.

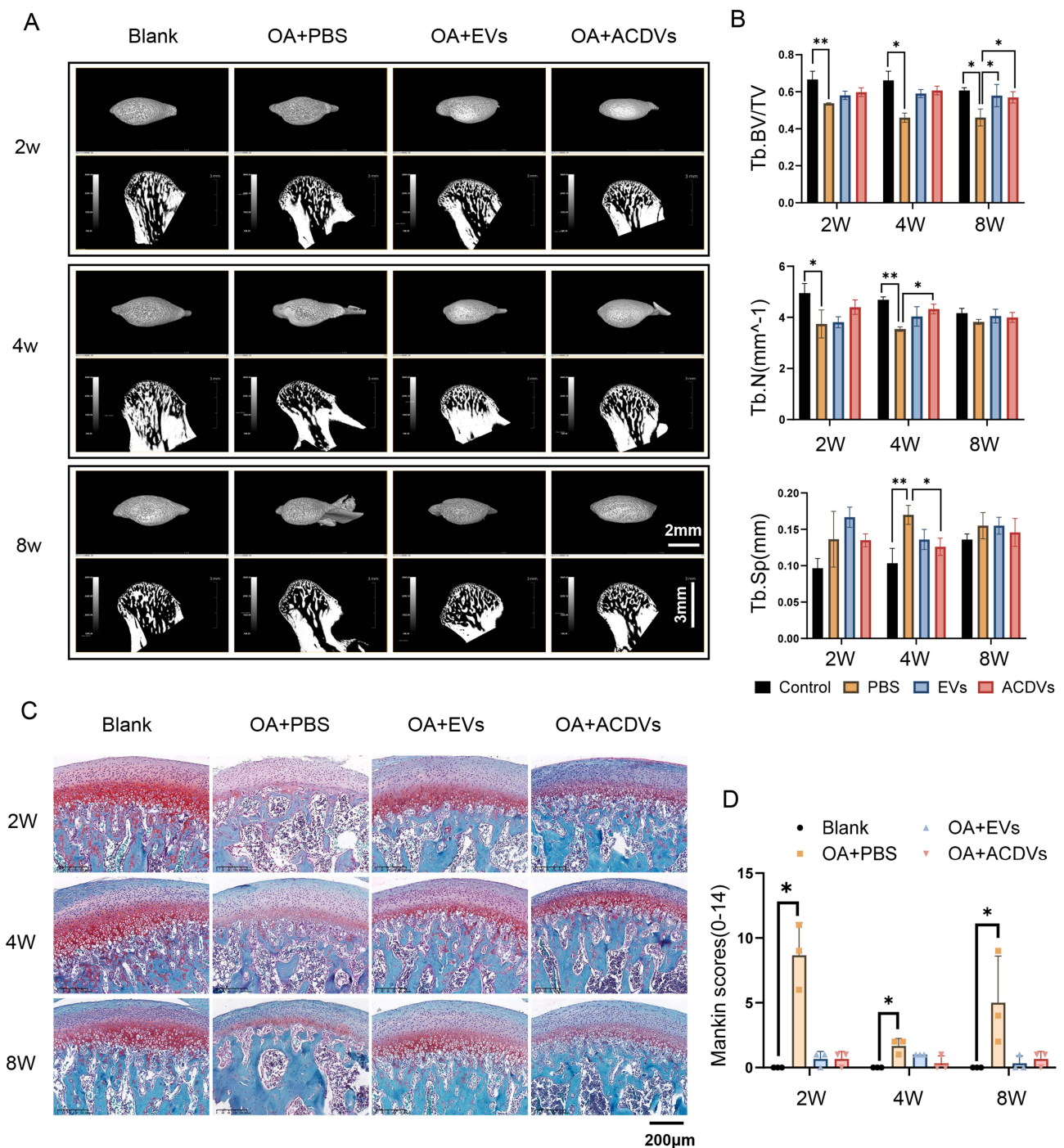


Figure 4 EVs and ACDVs promoted cartilage repair in TMJOA. **(A)** Micro-CT images of condylar samples. Scale bar = 2 mm; Scale bar = 3 mm. **(B)** Quantitative analysis of condylar bone parameters, including bone volume fraction (Tb.BV/TV), trabecular number (Tb.N), and trabecular spacing (Tb.Sp). $n = 3$. **(C)** Representative Safranin O/Alcian Blue staining images of condylar cartilage. **(D)** The Mankin score of condylar samples. $n = 3$. * $P < 0.05$; ** $P < 0.01$.

EVs and ACDVs Increased the sox9⁺ and COL2⁺ Cells in Damaged TMJ Cartilage

Immunohistochemistry revealed abundant sox9-positive nuclei in hypertrophic cells in the Blank group. At 8 weeks post-PBS injection in TMJOA rats, sox9 expression was reduced, while EVs and ACDVs treatment markedly restored sox9 levels, with the ACDVs group showing significant differences from PBS. Similarly, COL2 expression in condylar cartilage was substantially reduced in the PBS group, indicating impaired matrix synthesis, but was restored following EVs or ACDVs treatment (Figure 5A and B). These findings suggest that EVs and ACDVs can restore suppressed sox9 and COL2 expression in TMJOA.

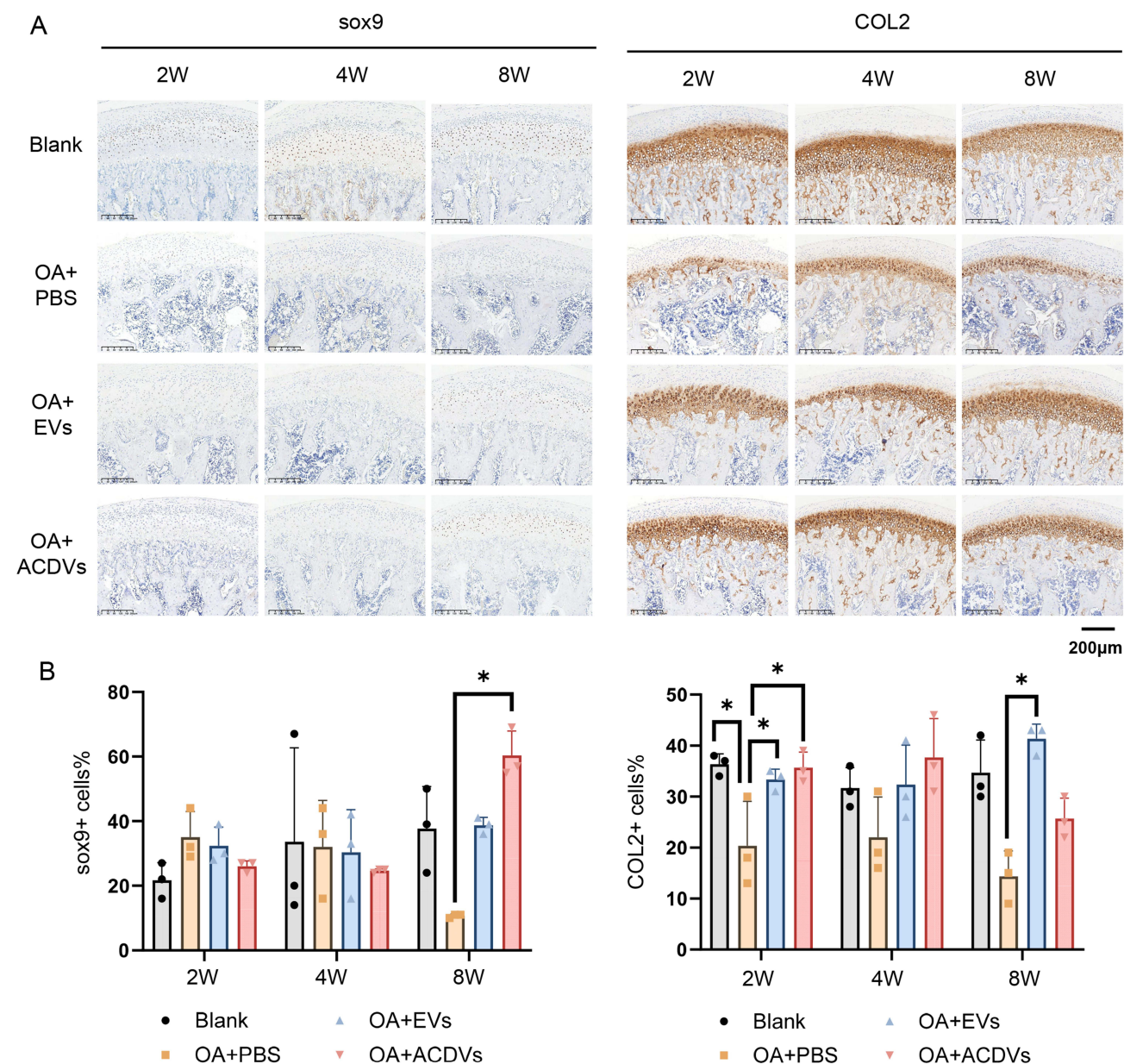


Figure 5 EVs and ACDVs enhanced cartilage matrix protein expression in TMJOA. **(A)** Immunohistochemical staining showing sox9 and COL2 expression in the condyle. Scale bar = 200 µm. **(B)** Quantitative analysis of sox9 and COL2 protein expression. n = 3. *P < 0.05.

Discussion

EVs hold therapeutic potential for osteoarthritis by modulating inflammation, maintaining homeostasis, and remodeling subchondral bone.^{23–25} However, limitations in EVs production and purification impede their clinical translation. As a promising alternative, engineered ACDVs offer both functional mimicry of EVs and high production efficiency, enabling potential use as carriers for nucleic acids and drugs. Here, we generated ACDVs via stepwise membrane extrusion, achieving vesicles with EV-like biological properties at significantly higher yields. Further studies showed that ACDVs promote the repair of articular cartilage and subchondral bone in TMJOA rat models by inhibiting chondrocyte apoptosis under inflammatory conditions, enhancing proliferation, and promoting chondrogenic differentiation.

In this study, ACDVs were produced from UCMSCs via stepwise membrane extrusion, resulting in ACDVs that share similar phospholipid bilayers and membrane proteins with EVs, thereby facilitating efficient internalization by host cells. Encouragingly, ACDVs exhibit comparable morphology, particle size, structural stability, and protein distribution to EVs,

yet with significantly higher particle numbers and protein yields. These findings provide a robust foundation for addressing the challenges of low yield and complex isolation associated with EVs. Notably, similar studies have demonstrated that stepwise membrane extrusion can produce ACDVs at over 20 times the yield of EVs.^{22,26} While MCC internalized both ACDVs and EVs rapidly, the uptake rate of ACDVs at 3 h was markedly higher. Whether it is attributed to non-selective extrusion process, potentially incorporating a broader spectrum of membrane proteins into ACDVs' phospholipid bilayer and thereby increasing their affinity for host cells—a hypothesis meriting further investigation. Previous studies have shown that extrusion-derived cell membrane vesicles possess a greater diversity of proteins compared to EVs from the same amount of parental cells.^{22,27} Moreover, proteomic analysis revealed that the protein composition and distribution of ACDVs are more closely aligned with those of the parent cells than EVs.²⁸

Chondrocyte apoptosis lies at the core of osteoarthritis pathogenesis.²⁹ Early in OA, apoptosis in the superficial and middle cartilage zones results in cell loss, which advances to deeper cartilage layers as the disease progresses.^{30,31} It remains unclear whether chondrocyte apoptosis is a driver of cartilage matrix degradation or a consequence of cartilage damage. Nonetheless, limiting excessive apoptosis and restoring chondrocyte populations are crucial for preserving extracellular matrix homeostasis.^{32,33} This study established an MCC inflammation model using 10 ng/mL IL-1 β , which elevated apoptosis and suppressed cartilage matrix synthesis, and broadly activated inflammatory pathways, including TNF, NF- κ B, and chemokines. Treatment with 50 μ g/mL ACDVs or EVs significantly reduced apoptosis and enhanced proliferation and migration. Notably, ACDVs rescued IL-1 β -induced inhibition of MCC chondrogenic differentiation, whereas EVs had no such effect. Transcriptomic analysis revealed that ACDVs significantly outperformed EVs in activating extracellular matrix genes, including *Tgfb1*, *Adamts1*, *Prg4*, and *Tgm2*. These results underscore ACDVs as a promising acellular therapeutic strategy, superior to EVs.³⁴ To model human TMJOA, we induced abnormal occlusal stress in rats through anterior crossbite, leading to TMJ dysfunction and subsequent TMJOA.^{35,36} Four weeks post-modeling, condylar bone displayed roughening, trabecular thinning, inflammatory cell infiltration, reduced chondrocyte density, and cartilage matrix degradation, confirming successful TMJOA induction. Similar models using unilateral anterior crossbite have closely recapitulated the progression and pathology of human TMJOA.^{37–41} Local injection of 50 μ g ACDVs reduced inflammatory infiltration in the condyle, restored cartilage integrity, upregulated COL2 and sox9 expression, and promoted subchondral bone remodeling.

Undoubtedly, this study has certain limitations and outstanding issues. While the stepwise extrusion method for preparing ACDVs is straightforward, the variability in protein load and quantity during extrusion may result in ACDV heterogeneity. Moreover, the tracking and retention time of ACDVs following local injection in the TMJOA rat model need further clarification. Additionally, while local inflammation is evident in this model, the potential for systemic inflammatory leakage warrants exploration. It is also important to assess whether ACDVs, while alleviating TMJ inflammation and repairing cartilage, may affect systemic immunity. Despite these unresolved issues, the findings provide a solid experimental foundation for the use of extruded cell-derived vesicles in temporomandibular and systemic osteoarthritis, and offer theoretical support for their application as carriers for nucleic acid and drug delivery.

Conclusion

This study shows that ACDVs, generated via stepwise extrusion, are produced in significantly higher yields than EVs and demonstrate equal or superior capabilities in cartilage matrix repair. ACDVs are effectively internalized by chondrocytes, mitigating inflammation-induced apoptosis while promoting proliferation, migration, and chondrogenic differentiation, ultimately restoring cartilage integrity in TMJOA rats. Additionally, ACDVs promote subchondral bone remodeling and stimulate cartilage matrix synthesis. These results provide strong experimental and theoretical support for ACDVs as a promising acellular therapeutic strategy, potentially surpassing EVs.

Abbreviations

ACDVs, artificial cell-derived vesicles; BCA, bicinchoninic acid; BV/TV, bone volume /tissue volume; COL2, type II collagen; DEGs, differentially expressed genes; EVs, extracellular vesicles; FBS, fetal bovine serum; HE, hematoxylin-eosin; IHC, Immunohistochemistry; MCCs, mandibular condylar chondrocytes; OA, Osteoarthritis; PBS, phosphate buffer solution; PCA,

Principal component analysis; Tb.N, trabecular number; Tb.Sp, trabecular separation; TEM, transmission electron microscopy; TMJOA, temporomandibular joint osteoarthritis; UCMSCs, umbilical mesenchymal stem cells.

Acknowledgments

This work was supported by the National Natural Science Foundation of China (Grant No. 82060206) and the First-Class Discipline Team of Kunming Medical University (Grant No. 2024XKTDTS09).

Disclosure

The authors report no conflicts of interest in this work.

References

1. Martel-Pelletier J, Barr AJ, Cicuttini FM, et al. Osteoarthritis. *Nat Rev Dis Primers*. 2016;2:16072. doi:10.1038/nrdp.2016.72
2. Hampton T. Improvements needed in management of temporomandibular joint disorders. *JAMA*. 2008;299(10):1119–1121. doi:10.1001/jama.299.10.1119
3. Li B, Guan G, Mei L, Jiao K, Li H. Pathological mechanism of chondrocytes and the surrounding environment during osteoarthritis of temporomandibular joint. *J Cell Mol Med*. 2021;25(11):4902–4911. doi:10.1111/jcmm.16514
4. Kim JY, Lee C, Park YL, Lee JH, Ryu YH, Huh JK. Diagnostic criteria for temporomandibular joint osteoarthritis using standardized uptake value in single-photon emission computed tomography-computed tomography. *Sci Rep*. 2024;14(1):31569. doi:10.1038/s41598-024-71639-1
5. Pantoja LLQ, de Toledo IP, Pupo YM, et al. Prevalence of degenerative joint disease of the temporomandibular joint: a systematic review. *Clin Oral Investig*. 2019;23(5):2475–2488. doi:10.1007/s00784-018-2664-y
6. de Souza RF, Lovato da Silva CH, Nasser M, Fedorowicz Z, Al-Muharraqi MA. Interventions for the management of temporomandibular joint osteoarthritis. *Cochrane Database Syst Rev*. 2012;2012(4):CD007261. doi:10.1002/14651858.CD007261.pub2
7. Arra M, Abu-Amer Y. Cross-talk of inflammation and chondrocyte intracellular metabolism in osteoarthritis. *Osteoarthritis Cartilage*. 2023;31(8):1012–1021. doi:10.1016/j.joca.2023.04.003
8. Yu H, Huang Y, Yang L. Research progress in the use of mesenchymal stem cells and their derived exosomes in the treatment of osteoarthritis. *Ageing Res Rev*. 2022;80:101684. doi:10.1016/j.arr.2022.101684
9. Nguyen TH, Duong CM, Nguyen XH, Than UTT. Mesenchymal stem cell-derived extracellular vesicles for osteoarthritis treatment: extracellular matrix protection, chondrocyte and osteocyte physiology, pain and inflammation management. *Cells*. 2021;10(11):2887. doi:10.3390/cells10112887
10. Liu L, Tang H, Wang Y. Nanotechnology-boosted biomaterials for osteoarthritis treatment: current status and future perspectives. *Int J Nanomed*. 2023;18:4969–4983. doi:10.2147/IJN.S423737
11. Yang X, Liu P, Zhang Y, Lu J, Zhao H. Bioprinting-enabled biomaterials: a cutting-edge strategy for future osteoarthritis therapy. *Int J Nanomed*. 2023;18:6213–6232. doi:10.2147/IJN.S432468
12. Kalluri R, LeBleu VS. The biology, function, and biomedical applications of exosomes. *Science*. 2020;367(6478):eaau6977. doi:10.1126/science.aau6977
13. Taghiyar L, Jahangir S, Khozaei Ravari M, Shamekhi MA, Eslaminejad MB. Cartilage repair by mesenchymal stem cell-derived exosomes: preclinical and clinical trial update and perspectives. In: *Advances in Experimental Medicine and Biology*. Springer; 2021:73–93.
14. Ye P, Mi Z, Wei D, Gao P, Ma M, Yang H. miR-3960 from mesenchymal stem cell-derived extracellular vesicles inactivates SDC1/Wnt/beta-Catenin axis to relieve chondrocyte injury in osteoarthritis by targeting PHLDA2. *Stem Cells Int*. 2022;2022:9455152. doi:10.1155/2022/9455152
15. Zhang S, Teo KYW, Chuah SJ, Lai RC, Lim SK, Toh WS. MSC exosomes alleviate temporomandibular joint osteoarthritis by attenuating inflammation and restoring matrix homeostasis. *Biomaterials*. 2019;200:35–47. doi:10.1016/j.biomaterials.2019.02.006
16. Guo P, Busatto S, Huang J, Morad G, Moses MA. A facile magnetic extrusion method for preparing endosome-derived vesicles for cancer drug delivery. *Adv Funct Mater*. 2021;31(44):2008326. doi:10.1002/adfm.202008326
17. Martínez-Santillán A, González-Valdez J. Novel technologies for exosome and exosome-like nanovesicle procurement and enhancement. *Biomedicine*. 2023;11(5):1487. doi:10.3390/biomedicine11051487
18. Li A, Zhao Y, Li Y, Jiang L, Gu Y, Liu J. Cell-derived biomimetic nanocarriers for targeted cancer therapy: cell membranes and extracellular vesicles. *Drug Deliv*. 2021;28(1):1237–1255. doi:10.1080/10717544.2021.1938757
19. Ren E, Liu C, Lv P, Wang J, Liu G. Genetically engineered cellular membrane vesicles as tailorable shells for therapeutics. *Adv Sci*. 2021;8(21):e2100460. doi:10.1002/advs.202100460
20. García-Manrique P, Gutiérrez G, Blanco-López MC. Fully artificial exosomes: towards new theranostic biomaterials. *Trends Biotechnol*. 2018;36(1):10–14. doi:10.1016/j.tibtech.2017.10.005
21. Ng CY, Kee LT, Al-Masawa ME, et al. Scalable production of extracellular vesicles and its therapeutic values: a review. *Int J Mol Sci*. 2022;23(14):7986. doi:10.3390/ijms23147986
22. Zhang Z, Mi T, Jin L, et al. Comprehensive proteomic analysis of exosome mimetic vesicles and exosomes derived from human umbilical cord mesenchymal stem cells. *Stem Cell Res Ther*. 2022;13(1):312. doi:10.1186/s13287-022-03008-6
23. Bertolino GM, Maumus M, Jorgensen C, Noël D. Therapeutic potential in rheumatic diseases of extracellular vesicles derived from mesenchymal stromal cells. *Nat Rev Rheumatol*. 2023;19(11):682–694. doi:10.1038/s41584-023-01010-7
24. Luo D, Zhu H, Li S, Wang Z, Xiao J. Mesenchymal stem cell-derived exosomes as a promising cell-free therapy for knee osteoarthritis. *Front Bioeng Biotechnol*. 2024;12:1309946. doi:10.3389/fbioe.2024.1309946
25. Wen S, Huang X, Ma J, et al. Exosomes derived from MSC as drug system in osteoarthritis therapy. *Front Bioeng Biotechnol*. 2024;12:1331218. doi:10.3389/fbioe.2024.1331218

26. Wang X, Hu S, Li J, et al. Extruded mesenchymal stem cell nanovesicles are equally potent to natural extracellular vesicles in cardiac repair. *ACS Appl Mater Interfaces*. 2021;13(47):55767–55779. doi:10.1021/acsami.1c08044
27. Nasiri Kenari A, Kastaniegaard K, Greening DW, et al. Proteomic and post-translational modification profiling of exosome-mimetic nanovesicles compared to exosomes. *Proteomics*. 2019;19(8):e1800161. doi:10.1002/pmic.201800161
28. Liang L, Wang L, Liao Z, et al. High-yield nanovesicles extruded from dental follicle stem cells promote the regeneration of periodontal tissues as an alternative of exosomes. *J Clin Periodontol*. 2024;51(10):1395–1407. doi:10.1111/jcpe.14036
29. Castrogiovanni P, Ravalli S, Musumeci G. Apoptosis and autophagy in the pathogenesis of osteoarthritis. *J Invest Surg*. 2020;33(9):874–875. doi:10.1080/08941939.2019.1576811
30. Liu Z, Wang T, Sun X, Nie M. Autophagy and apoptosis: regulatory factors of chondrocyte phenotype transition in osteoarthritis. *Hum Cell*. 2023;36(4):1326–1335. doi:10.1007/s13577-023-00926-2
31. Hosseinzadeh A, Kamrava SK, Joghataei MT, et al. Apoptosis signaling pathways in osteoarthritis and possible protective role of melatonin. *J Pineal Res*. 2016;61(4):411–425. doi:10.1111/jpi.12362
32. Theocharis AD, Skandalis SS, Gialeli C, Karamanos NK. Extracellular matrix structure. *Adv Drug Deliv Rev*. 2016;97:4–27. doi:10.1016/j.addr.2015.11.001
33. Walma DAC, Yamada KM. The extracellular matrix in development. *Development*. 2020;147(10):dev175596. doi:10.1242/dev.175596
34. Jang HJ, Shim KS, Lee J, et al. Engineering of cell derived-nanovesicle as an alternative to exosome therapy. *Tissue Eng Regen Med*. 2024;21(1):1–19. doi:10.1007/s13770-023-00610-4
35. Cai S, Zou Y, Zhao Y, et al. Mechanical stress reduces secreted frizzled-related protein expression and promotes temporomandibular joint osteoarthritis via Wnt/beta-catenin signaling. *Bone*. 2022;161:116445. doi:10.1016/j.bone.2022.116445
36. Qi H, Zhang Y, Xu L, et al. Loss of RAP2A aggravates cartilage degradation in TMJOA via YAP signaling. *J Dent Res*. 2023;102(3):302–312. doi:10.1177/00220345221132213
37. Chen BY, Pathak JL, Lin HY, et al. Inflammation triggers chondrocyte ferroptosis in TMJOA via HIF-1alpha/TFRC. *J Dent Res*. 2024;103(7):712–722. doi:10.1177/00220345241242389
38. He F, Ma Y, Li S, et al. Necroptotic TNFalpha-Syndecan 4-TNFalpha vicious cycle as a therapeutic target for preventing temporomandibular joint osteoarthritis. *J Bone Miner Res*. 2022;37(5):1044–1055. doi:10.1002/jbmr.4542
39. Qi H, Zhao Z, Xu L, et al. Antisense oligonucleotide-based therapy on miR-181a-5p alleviates cartilage degradation of temporomandibular joint osteoarthritis via promoting SIRT1. *Front Pharmacol*. 2022;13:898334. doi:10.3389/fphar.2022.898334
40. Zhu M, Huang Z, Qin J, Jiang J, Fan M. Loss of beta-arrestin2 aggravated condylar cartilage degeneration at the early stage of temporomandibular joint osteoarthritis. *BMC Musculoskelet Disord*. 2024;25(1):451. doi:10.1186/s12891-024-07558-z
41. Wei JM, Tu SQ, Wang YX, et al. Clock gene Per1 regulates rat temporomandibular osteoarthritis through NF-kappaB pathway: an in vitro and in vivo study. *J Orthop Surg Res*. 2023;18(1):817. doi:10.1186/s13018-023-04301-7

International Journal of Nanomedicine

Publish your work in this journal

The International Journal of Nanomedicine is an international, peer-reviewed journal focusing on the application of nanotechnology in diagnostics, therapeutics, and drug delivery systems throughout the biomedical field. This journal is indexed on PubMed Central, MedLine, CAS, SciSearch®, Current Contents®/Clinical Medicine, Journal Citation Reports/Science Edition, EMBase, Scopus and the Elsevier Bibliographic databases. The manuscript management system is completely online and includes a very quick and fair peer-review system, which is all easy to use. Visit <http://www.dovepress.com/testimonials.php> to read real quotes from published authors.

Submit your manuscript here: <https://www.dovepress.com/international-journal-of-nanomedicine-journal>

Dovepress
Taylor & Francis Group